Available online at www.sciencedirect.com
ScienceDirect
Earth and Planetary Science Letters 264 (2007) 266–276
EPSL
www.elsevier.com/locate/epsl

The fate of the Juan de Fuca plate: Implications for a Yellowstone plume head

Mei Xue, Richard M. Allen *

Department of Earth and Planetary Science, University of California Berkeley, USA

Received 22 March 2007; received in revised form 25 September 2007; accepted 29 September 2007
Available online 13 October 2007
Editor: R.D. van der Hilst

Abstract

Beneath the Pacific Northwest the Juan de Fuca plate, a remnant of the Farallon plate, continues subducting beneath the North American continent. To the east of the Cascadia subduction zone lies the Yellowstone Hotspot Track. The origins of this track can be traced back to the voluminous basaltic outpourings in the Columbia Plateau around 17 Ma. If these basalts are the result of a large melting anomaly rising through the mantle to the base of the North American continent, such as a mantle plume head, the anomaly would need to punch through the subducting Juan de Fuca slab. Here, we use teleseismic body-wave travel-time tomography to investigate the fate of the subducted slab and its possible interaction with a plume head. Our dataset is derived from the Oregon Array for Teleseismic Study (OATS) deployment in Oregon and all other available seismic data in this region during the same period. In our JdF07 models, we image the subducted Juan de Fuca plate in the mantle east of the Cascades beneath Oregon, where the slab has not been imaged before, to a depth of 400 km but no deeper. The slab dips ~50°E and has a thickness of ~75 km. Immediately beneath the slab, we image a low velocity layer with a similar geometry to the slab and extending down to at least ~575 km depth in the V_s model. The total length of the high velocity slab is ~660 km, about 180 km longer than the estimated length of slab subducted since 17 Ma. Assuming similar slab geometry to today, this 180 km length of slab would reach ~60 km depth, comparable to the thickness of continental lithosphere. We propose that the absence of the slab below 400 km today is due to the arrival of the Yellowstone plume head ~17 Ma, which destroyed the Juan de Fuca slab at depths greater than the thickness of the continental lithosphere. Given this scenario, the low velocity anomaly beneath the slab is likely the remnant plume head material which has been pulled down by traction with the subducting plate. The amplitude of the observed low velocity anomaly is comparable with that expected for plume head material 100–300 °C hotter than the surrounding asthenosphere.

Keywords: Juan de Fuca Plate; Yellowstone plume head; Oregon; body-wave tomography; Cascadia subduction

1. Introduction

In the Pacific Northwest, the Juan de Fuca plate is currently subducting beneath the northwestern United States and southwestern Canada (Fig. 1). Due to its proximity to the Juan de Fuca Ridge to the west, the Juan de Fuca plate being subducted is young ~10 Ma old (Severinghaus and Atwater, 1990) and thus thin and

* Corresponding author. Department of Earth and Planetary Science, University of California Berkeley, 307 McCone Hall, Berkeley, CA 94720-4767, USA. Tel.: +1 510 642 1275; fax: +1 510 643 5811.
E-mail address: rallen@berkeley.edu (R.M. Allen).

0012-821X/$ - see front matter © 2007 Elsevier B.V. All rights reserved.
doi:10.1016/j.epsl.2007.09.047

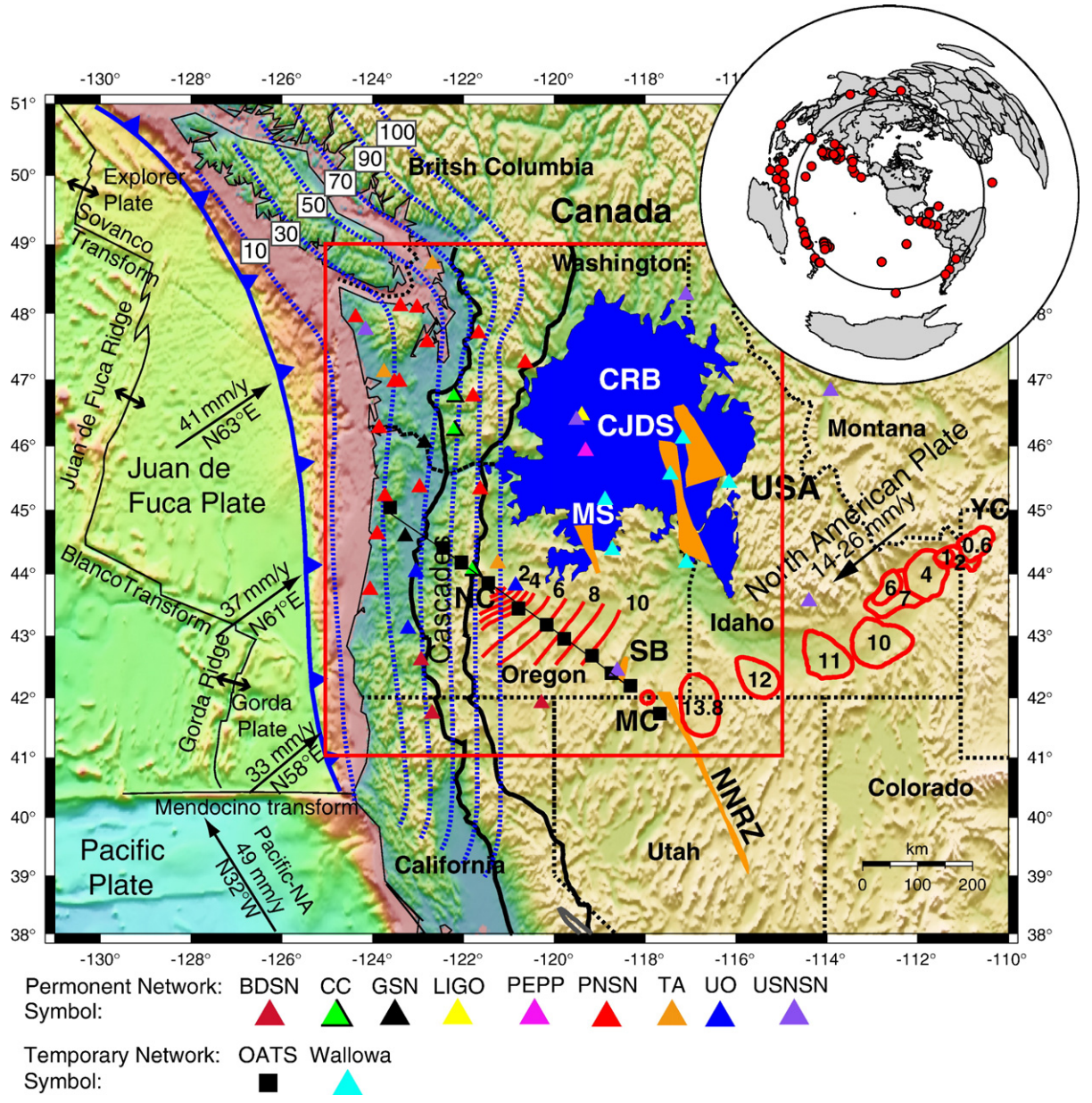

Fig. 1. Tectonic map for the study region. Plate motions from HS3-NUVEL 1A are shown as black arrows (Gripp and Gordon, 2002). Blue dotted lines show the depth contours of the Juan de Fuca slab (McCrory et al., 2006). The thick black lines delineate the Cascade Range. Age contours of initial rhyolitic volcanism along the Newberry track are shown in 1 Ma increments extending to the Newberry Caldera (NC) (Jordan et al., 2004). Major rhyolitic caldera centers along the Yellowstone track are shown with age in Ma extending to the Yellowstone Caldera (YC) (Pierce and Morgan, 1992). Both tracks initiate in the region of the McDermitt Caldera (MC), which is shown as a red circle. The Columbia River Basalt is shown in blue (12 to 17 Ma) (Christiansen et al., 2002). Dike swarms associated with the 17 Ma basaltic outpourings are shown in gold (Camp and Ross, 2004; Christiansen and Yeats, 1992): Chief Joseph Dike Swarm (CJDS), Monument Swarm (MS), Steens Basalt (SB), and Northern Nevada Rift Zone (NNRZ). The seismic stations used in this study are shown as triangles and squares with a total number of 52. Inset shows the distribution of the 95 events used in the inversion for the S-wave velocity model. The red square outlines the study region. The thick black line across OATS array indicates the location of the cross-section shown in Figs. 2 and 3.

warm. The relative youth of the plate may be the cause of some of the unusual characteristics of this subduction zone. There is very little seismicity associated with the slab and a clear Wadati–Benioff zone of earthquakes is lacking compared to other subduction zones (e.g. Shelly et al., 2006; Zhao et al., 1995). The Juan de Fuca plate is a remnant of the Farallon plate. Around 30 Ma, when the ridge separating the Farallon and Pacific plates reached

the North American plate, the Pacific and North American Plates began to interact (Severinghaus and Atwater, 1990). The Farallon plate was split into two major subplates, and the Juan de Fuca plate is the central part of the northern sub-plate.

To the east of the Juan de Fuca subduction system are the Columbia River Basalts, the Yellowstone Hotspot Track and the High Lava Plains of Oregon, also referred as the Newberry Hotspot Track (Fig. 1). The Columbia River basalts extend throughout eastern Oregon, eastern Washington, and western Idaho, and are a series of flows with ages primarily 17–14 Ma (e.g., Camp and Ross, 2004; Christiansen et al., 2002). The conduits for these flows lie along a NS-oriented trend, north of the McDermitt Caldera (Chief Joseph Dike Swarm and Monument Swarm) and similar NS-oriented trends of magmatism occur southward at Steens Basalt dike and along the Northern Nevada rift zone (Fig. 1). The Newberry Hotspot Track, along the Oregon High Lava Plains, consists of a sequence of volcanic domes and lava flows. Isochrones of rhyolitic domes show a monotonic age progression from east to west ending at the Newberry Caldera (Fig. 1) (Jordan, 2005). The Yellowstone Hotspot Track is associated with northeastward migration of silicic volcanism along the Eastern Snake River Plain ending at the Yellowstone Caldera (e.g., Pierce and Morgan, 1992; Smith and Braile, 1994) (Fig. 1). The Newberry and Yellowstone tracks show age-progressive volcanism migrating away from a region near McDermitt Caldera which was first active around ~17 Ma. One interpretation for the voluminous basaltic outpourings of Columbia River Basalts, Steens Basalts, Chief Joseph Dike Swarm and Northern Nevada Rift Zone, and the formation of the Yellowstone Hotspot Track is that a mantle plume impacted the North America lithosphere around 17 Ma. In this model, the tail of the plume is responsible for the Yellowstone track as the absolute plate motion of North American Plate is in a southwesterly direction. This is consistent with the associated gravity high, topographic high, high heat flow, and geochemical signature, which are characteristics of many hotspots. Yet, despite these features, evidence for an upwelling conduit through the upper mantle beneath Yellowstone remains unclear and the debate continues as to whether a mantle plume is the origin (e.g., Humphreys et al., 2000; Jordan et al., 2004; Waite et al., 2006; Yuan and Dueker, 2005). Given the proximity of the slab and the proposed Yellowstone plume it is likely that the subduction and the upwelling processes interact with one another (e.g., Geist and Richards, 1993; Pierce et al., 2000).

A considerable amount of geophysical data illuminates the subducting Juan de Fuca plate west of the Cascades, e.g. controlled source reflection and refraction data offshore Washington and Oregon (e.g., Flueh et al., 1998; Trehu et al., 1995) and teleseismic scattered waves in northern Oregon (Bostock et al., 2002). These studies provide clear evidence that the oceanic crust of the subducting Juan de Fuca plate is dipping at a few degrees with a steadily increasing dip to the east reaching ~10° beneath the Coastal Ranges, and ~30° beneath the Cascades. The andesitic volcanism of the Cascade Mountains also provides independent evidence for the presence of a slab. However, previous tomographic studies suggest that the slab is not ubiquitous at greater depths east of the Cascades. In the northernmost part, the slab has been imaged to depths of ~400 to 500 km beneath British Columbia with a dip averaging 50° to the northeast (Bostock and VanDeckar, 1995). Beneath northern and central Washington, the slab has been imaged to a depth of ~300 to 400 km with a steeper dip of 60° to 65° to the east (Bostock and VanDecar, 1995; Rasmussen and Humphreys, 1988) or a shallower dip of 45° to the east–northeast (Michaelson and Weaver, 1986). Further south beneath southern Washington and northern Oregon, the imaged slab extends to ~300 km depth dipping 60° to the east (Michaelson and Weaver, 1986). However, further south beneath Oregon, the slab has only been imaged to a depth of ~150 km with an apparently vertical dip beneath the Cascades (Rasmussen and Humphreys, 1988). At the southernmost part of the subduction zone beneath southern Oregon, the imaged slab extends down to a depth of ~200 km beneath the Cascade Range dipping ~65° to the east along a NW–SE array across southern Oregon (Harris et al., 1991).

Although the slab has been imaged to depths of ~300 to 400 km beneath Washington, there is little evidence for the presence of a slab in the mantle east of the Cascades beneath Oregon (Bostock et al., 2002; Harris et al., 1991; Michaelson and Weaver, 1986; Rasmussen and Humphreys, 1988). The question, therefore, is does the Juan de Fuca slab extend down deeper into the mantle east of the Cascades beneath Oregon, or does it break up and disintegrate due to its young age or the passage of the proposed Yellowstone plume? The apparent absence of the slab east of the Cascades has been interpreted as suggesting that (1) the slab has a small velocity contrast making the slab indistinct from the surrounding mantle (Michaelson and Weaver, 1986), (2) the slab has a vertical geometry (Rasmussen and Humphreys, 1988) or has broken off with a steep dip (Michaelson and Weaver, 1986; Rasmussen and Humphreys, 1988), or (3) a loss of seismic resolution prevents imaging of the slab (Rasmussen and Humphreys, 1988). Here, we present

new seismic tomographic models JdF07-S and JdF07-P that answer these questions by mapping the Juan de Fuca slab into the mantle to a depth of ~400 km east of the Cascades beneath Oregon but no deeper.

2. Data and method

We use a dataset collected from the Oregon Array for Teleseismic Study (OATS) that was deployed in May 2003 and operated until May 2006. The OATS array includes eleven 3-component broadband seismic stations (Guralp CMG-3ESPD) with an average station spacing of 50 km. The permanent station COR at Corvallis represents a twelfth station. The OATS array extends northwest–southeast across Oregon from the coast to the McDermitt Caldera (Fig. 1). The dataset from OATS was complemented by data from 9 permanent networks and a temporary deployment as shown in Fig. 1. The nine permanent networks are the Berkeley Digital Seismograph Network (BDSN), Cascade Chain Volcano Monitoring (CC), Global Seismograph Network (GSN), Laser Interferometer Gravitational-Wave Experiment (LIGO), Princeton Earth Physics Project-Indiana (PEPP), Pacific Northwest Regional Seismic Network (PNSN), USArray Transportable Network (TA), University of Oregon Regional Network (UO), and the United States National Seismic Network (USNSN). The temporary deployment is the Wallowa Mountains Experiment. A total of 52 stations were used. The data from seismic events with epicentral distance greater than 30° and magnitude 6.0 and above from July 19th, 2003 to Nov. 10th, 2004 were inspected for all stations. For the S-velocity inversion, a total of 95 events (Fig. 1) with clear S and SKS phases were recorded at 45 stations and a total of 2148 rays were used. For the P-velocity inversion, a total of 78 events with clear P and PKiKP phases were recorded at 46 stations and a total of 2101 rays were used. As the interference of phases at some epicentral distances can bias the relative arrival times determined using cross-correlation, such as P and PcP at 80°–90°, PKIKP and PKiKP at 120°–144°, we discarded most events which fall into above epicentral distances and only include events with clearly separated phases.

We follow a similar inversion procedure as described in Allen et al. (2002). We manually check each waveform and pick either the first valley or the first peak. All the arrivals were picked by hand initially. The arrivals are then cross-correlated to obtain relative arrival times between all pairs of stations for each event (Vandecar and Crosson, 1990). The average standard deviation of the relative travel times determined from cross-correlation is 0.05 s for S and 0.02 s for P. The average cross-correlation coefficient is 0.89 for S and 0.86 for P. Rather than reference relative arrival times to an absolute arrival time pick, we set the average relative arrival time of each event to zero. The consequence of this approach is the loss of absolute travel time, preventing recovery of velocity anomalies common to all ray paths.

We analyzed the noise for OATS stations in December of 2003, and February, July, and October of 2004 and found that the noise peaks from 0.13–0.3 Hz. To avoid the possible influence of noise as well as observe the arrivals clearly, S and SKS arrivals were picked and cross-correlated in the frequency window of 0.02–0.1 Hz; and P arrivals were processed in the frequency window of 0.8–2.0 Hz. For cross-correlation, we chose a window length equal to approximately one wavelength or less for the arrivals observed in each frequency window, which is 10 s for S and SKS and 1.25 s for P and PKiKP respectively.

The dimension of the model space is 1000 × 1000 × 1000 km, centered at 45°N and 119.375°W. The model grid spacing and the smoothing length are 25 km and 40 km respectively in all three directions. The region parameterized is more expansive than the volume in which we expect to resolve structure in order to ensure that anomalies are not compressed into the model box.

To account for the local structure beneath each station and accommodate any baseline shift between the relative travel-time sets for different events, station corrections and event corrections were included respectively in the inversion. For the S- and P-wave velocity models, a damping factor of 0.2 was used and a priori standard deviations of 3%, 0.6 s, and 0.5 s were used for the velocity nodes, station corrections, and event corrections respectively. Different values were tested and variations in these parameters of a factor of 2 or 3 had little effect on the inversion results. For S-wave velocity models, the initial RMS residual is 1.20 s and after inversion, the RMS is reduced to 0.54 s, a var reduction of 54%. For P-wave velocity models, after inversion, the RMS residual is reduced from the initial 0.57 s to 0.30 s and the var reduction is 46%.

3. Tomographic results and resolution tests

Here we present the vertical slices through our S- and P-wave velocity models (JdF07-S and JdF07-P respectively, hereafter referred to as V_s and V_p models) along the OATS array where both models have the highest resolution, as shown in Fig. 2a and b. The most prominent feature in our tomographic models is the high velocity anomaly which dips ~46° and extends down to a depth of ~400 km. We interpret this feature as the subducted Juan de Fuca plate. The cross-section is not perpendicular to the trench which is approximately

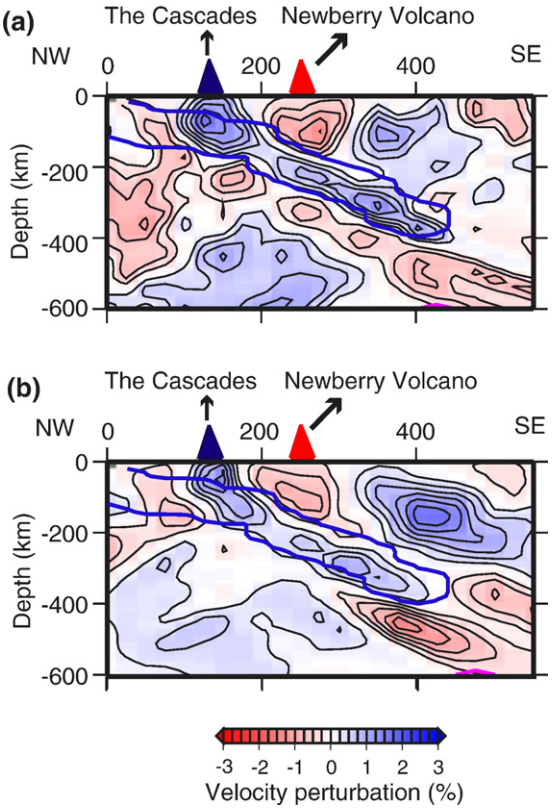

Fig. 2. Vertical slices through the (a) JdF07-S and (b) JdF07-P models along the OATS line indicated in Fig. 1. The envelope of the synthetic slab ending at 400 km depth as shown in Fig. 3 (c) is shown by the blue outline. The contour interval is 0.25% indicated by vertical lines in the color bar of the velocity scale. Zero contours are not shown. The locations of the Cascades and the Newberry Volcano are shown as blue and red triangles respectively.

north–south oriented. Instead the cross-section is rotated 28° clockwise from the trench-perpendicular direction. After correcting for the oblique trend of the cross-section, the dip angle of the slab is 50° to the east.

The second prominent feature is the low velocity body beneath the slab in the V_s model, though this feature is not as evident in the V_p model. Other features observed are a low velocity anomaly beneath the Newberry volcano, and to its immediate SE a shallow high velocity anomaly. These features are visible in both V_s and V_p models, though their geometry differs a little in the two models.

The better ray coverage available from shear-wave arrivals means the V_s model has greater resolution than the V_p model. We therefore focus on the V_s model and present several resolution tests to assess the reliability of the prominent features. First, we conducted a checkerboard sensitivity test using alternating anomalies of high and low velocities evenly spaced throughout the model to a depth of 525 km in a 3D checkerboard pattern. Each anomaly has the geometry of a cylinder with a vertical axis and a dimension of 100 km in both the vertical and horizontal directions. In the vertical direction, we put four alternating velocity anomalies centered at depths of 100, 225, 350, and 475 km respectively. Fig. 3a shows a vertical slice along the OATS array through the input model and Fig. 3b shows the recovered velocity anomalies. The size and shape of the anomalies are preserved well in the upper and middle sections of the model, i.e. in a triangular region beneath the OATS array. We recover two thirds of the input anomaly amplitudes. Outside the triangular region in the bottom corners of the model, the anomalies are smeared. All the velocity model features discussed in this paper are within the well-resolved triangular region.

Next we conducted realistic anomaly recovery tests on the observed slab feature as shown in Fig. 3c, d, e, and f. These tests explore how well our dataset can resolve a slab at different depths. At greater depth, the dip angle of all synthetic slab is 50° to the east, the same as imaged in this study. The shallow and nearly horizontal portion of the synthetic slab is based on the observed shallow slab structure in a previous study in northern Oregon (Bostock et al., 2002). As demonstrated in the resolution tests, our dataset cannot resolve the shallow nearly horizontal portion of the slab (Fig. 3d, e, and f). The reason is that we use teleseismic events for which rays have near vertical ray paths beneath stations. For horizontal structures near the Earth surface, the lengths of ray segments passing through such structures are almost identical and so are their contributions to travel-time delays. As we use relative travel times, any common contributions would cancel out, making them difficult to image. Fig. 3c shows an input slab extending down to 400 km and the corresponding inversion result is shown in Fig. 3d. In this case, the recovered structure closely resembles the observed slab feature. In Fig. 3e, the synthetic slab extends down to only 300 km depth. The inversion result shows that a slab ending at 300 km depth does not smear significantly down dip and is not sufficient to produce the observed slab structure between 300 km and 400 km depth.

To test whether the slab extends to depths greater than 400 km, we conducted the test shown in Fig. 3f where the input slab extends down to 500 km depth. We conclude that the Juan de Fuca slab does not extend to depths greater than 400 km. This is because the recovered structure in our resolution test differs from the observed structure between 400 and 500 km depth in two aspects: (1) the recovered anomaly in the resolution test shows a strong velocity anomaly to 500 km depth

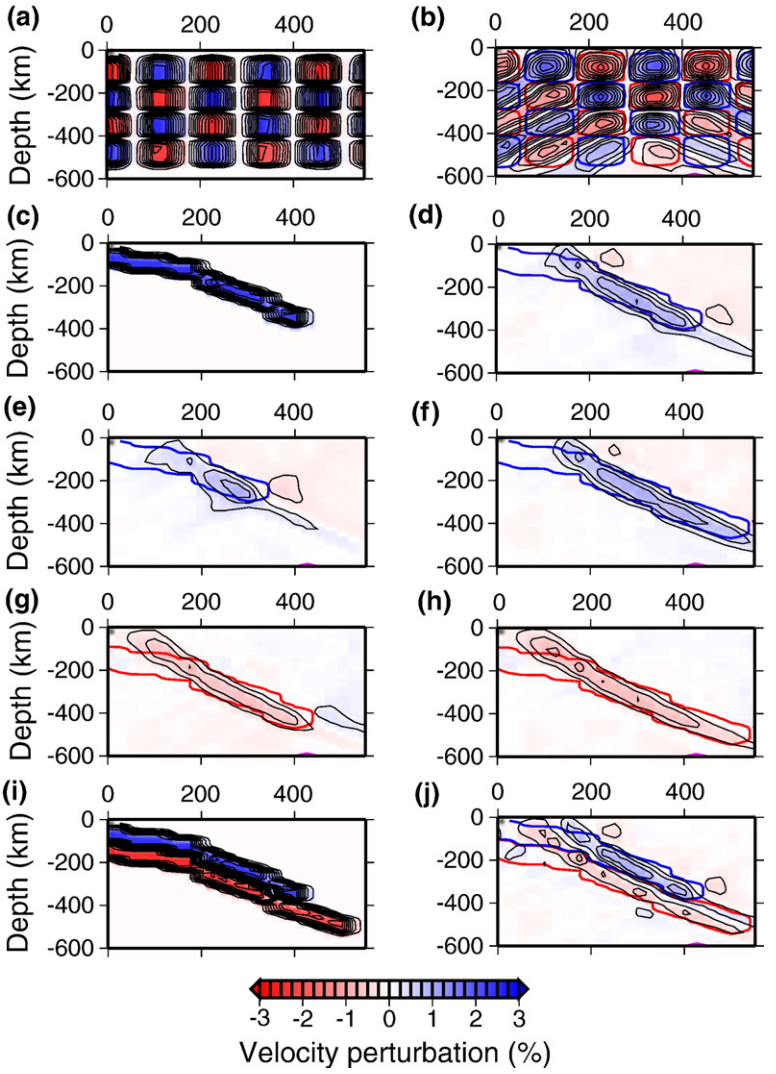

Fig. 3. Resolution tests for the JdF07-S V_s velocity model. All slices are along the OATS line as in Fig. 2. (a) The input model of the checkerboard test and (b) the recovered model. (c) A synthetic slab ending at 400 km and (d) the recovered model. The recovered models for a slab ending at 300 km and 500 km depth are shown in (e) and (f) respectively. The recovered model for a low velocity body to 475 km and 575 km depth are shown in (g) and (h) respectively. (i) The synthetic model with a slab ending at 400 km depth and a low velocity anomaly body underneath ending at 575 km depth and (j) the recovered model. The amplitude of the input V_s anomaly is 3%. Input models are overlain on the recovered models by thick lines with blue for high velocity anomaly and red for low velocity anomaly. The contour interval and color scale are the same as in Fig. 2.

while the observed anomaly does not extend to 500 km depth, (2) the transition of velocity anomaly from higher amplitudes to lower amplitudes along the length of the slab in the recovered structure is smooth along the length of the slab, unlike the step-like transition we observe in our model.

We also conducted realistic anomaly recovery tests on the observed low velocity body underneath the slab as shown in Fig. 3g and h. These tests explore if our dataset can resolve such a low velocity body and how well it can be resolved at different depths. We use the same geometry for the synthetic low velocity body as that for the slab. Fig. 3g shows the recovered velocity structure for a synthetic low velocity body extending down to 475 km depth. The geometry of the input anomaly is very well resolved with insignificant smearing essentially close to zero. For a low velocity body extending deeper to 575 km depth, our dataset also resolves the geometry well with only minor smearing about 50 km along the slab as shown in Fig. 3h.

However, the amplitude is only partially recovered in both cases. These tests demonstrate that our dataset is able to resolve this feature down to a depth of 575 km.

For a synthetic velocity structure consisting of a slab extending down to 400 km depth and a low velocity layer beneath the slab extending to 575 km depth (Fig. 3i), the locations and geometries of the recovered the high velocity slab and the low velocity body underneath (Fig. 3j) are very similar to what we observed (Fig. 2a) but with a reduced amplitude, about two thirds of what we observed. Based on our velocity model images and resolution tests, we propose that the true Earth structure consists of a slab extending down to ~400 km depth with a low velocity body beneath extending to at least 575 km depth. While we conclude that the high velocity slab does not extend deeper than ~400 km, the low velocity feature may extend deeper than 575 km.

4. Discussion

We interpret the high velocity anomaly dipping eastward into the mantle as the subducted Juan de Fuca plate. The observed velocity contrast is likely largely due to the temperature contrast between the slab and the surrounding mantle as temperature anomalies have a greater velocity signature than composition in the upper mantle (Goes et al., 2000). The observed dip of 50° is similar to, but a little shallower, than other portions of the slab to the north and south of Oregon, where the slab dip has been constrained as ~60° to 65° to the east (Harris et al., 1991; Michaelson and Weaver, 1986; Rasmussen and Humphreys, 1988).

Though previous studies have speculated that the portion of the Juan de Fuca slab beneath Oregon might have a smaller velocity contrast than that to the north (Michaelson and Weaver, 1986; Rasmussen and Humphreys, 1988), the amplitude of the dipping high velocity anomalies are similar in our model beneath both Washington and Oregon (not shown). The maximum velocity contrast we observed for the slab below 100 km depth is 1.25% in the V_s model and 0.75% in the V_p model. These values are likely smaller than the real amplitudes as not all of the anomaly amplitude is recovered during the inversion due to smoothing, damping, and imperfect ray coverage. Our resolution tests show that, for a synthetic slab with 3% high velocity anomaly, the percentage of recovery under our inversion scheme is about ~30% for V_s and ~40% for V_p. Thus we expect that the true velocity anomaly associated with the slab is approximately 3 times stronger for V_s and 2.4 times stronger for V_p than what we recovered, i.e. around ~3.8% for V_s and 1.8% for V_p. When compared to the 3–4% V_p anomalies observed in old subduction zones such as Tonga, Izu–Bonin, Japan, and Kuril subduction zones (Deal and Nolet, 1999; Deal et al., 1999), the ~2% V_p anomaly we observed for the slab in central Oregon is low. This suggests that the Juan de Fuca plate is warm, likely due to its relatively young age ~10 Ma (Severinghaus and Atwater, 1990).

The amplitude of the high velocity anomaly is greatest immediately beneath the Cascades in both our V_s and V_p models (Fig. 2a and b). Resolution tests show that this is unlikely to be an artifact of the inversion, indicating the presence of high velocities beneath the Cascades. As any contributions to the velocity models from the crust would be greatly reduced by station correction, the significant increase in high velocity anomalies implies the uppermost mantle has anomalously high velocity. This is likely the result of mantle melts leaving a depleted residuum behind.

Does the slab go deeper than 400 km depth? As the slab descends into the mantle, it is warmed and the surrounding mantle cools. The subduction rate of the Juan de Fuca plate ranges from 33 mm/yr to 41 mm/yr from northern California to central Washington (Gripp and Gordon, 2002). For a 60° dipping slab with this rate of subduction the temperature anomaly of the slab would be between 200 and 400 °C colder than the surrounding mantle in a region 80 km wide at depths greater than 400 km (i.e. 8 Ma to 22 Ma since subduction) (Davies and Stevenson, 1992). As every 100 °C decrease in temperature results in an increase of ~1% in the S-wave velocity (Cammarano et al., 2003), we expect the slab at depths greater than 400 km to have high S-velocity anomalies of ~2% to 4% which should be easily resolved. This warming effect would also generate a gradual velocity contrast between the slab and the surrounding mantle. Instead, we see an abrupt end to the down-dip edge of the imaged slab (Fig. 2a and b). Resolution tests also indicate that we would image any slab to depth of ~600 km if it was present (Fig. 3d, e, and f). Thus if the slab is present at depths greater than 400 km, we would be able to resolve it. Therefore, we suggest that the slab ends at 400 km depth. Then the question becomes: what caused the abrupt end of the slab at 400 km depth given that there has been subduction in this region for the last 150 million years.

It has been proposed that a mantle plume head impacted near the McDermitt Caldera and caused the initiation of broad volcanism throughout the region at ~17 Ma (e.g., Draper, 1991; Pierce et al., 2000). For such a plume to reach the base of the lithosphere it would have to punch through the subducting Juan de Fuca slab blocking the path of the plume to the surface. This would have created a lower edge to the subducted slab which would then continue to subduct deeper into

the mantle for the last ~17 Ma. The subduction rate of the Juan de Fuca plate is estimated to be 33 mm/yr N58°E near the trench west of southern Oregon for the last ~6 Ma (Gripp and Gordon, 2002). The east component of this subduction rate, perpendicular to the trench, is 28 mm/yr. As the average plate speed has remained fairly constant since 19 Ma (Wilson, 1988), we can use this value to estimate the amount of oceanic lithosphere subducted to the east since 17 Ma. The estimated total length of slab subducted to the east in the last 17 Ma is ~480 km. Using our imaged slab (Fig. 2a and b) we can measure the length of the observed slab from the present trench in an east–west direction. The total length of imaged slab is ~660 km. This means that at 17 Ma, the bottom edge of the slab we observe today would be at the end of a 180 km length of subducted slab. Assuming that the slab geometry was similar to today, the end of the slab we observe would be at ~60 km depth given the shallow dip of the slab from the trench to the Cascades. While the thickness of the North American lithosphere is uncertain, the 60 km depth of the end of the slab is likely comparable to the thickness of the lithosphere. Thus, the absence of the slab at greater depths could be explained by a plume head destroying a large portion of the Juan de Fuca slab, potentially all of the slab at depths greater than the thickness of the continental lithosphere.

Unfortunately global and continental scale velocity models typically do not have the resolution to image structures on the scale of those discussed here (e.g., Bijwaard et al., 1998; Grand, 2002; Marone and Romanowicz, 2007). However, vanderLee and Nolet (1997) imaged a high velocity anomaly above 400 km depth beneath Cascadia, but they do not image this high velocity anomaly extending down into the transition zone from 410 km to 660 km depth. This is in contrast to the clear evidence for the Farallon slab in the transition zone to the south of Cascadia where a continuous high velocity anomaly is observed from northern California to central America (vanderLee and Nolet, 1997). While the resolution in Van der Lee and Nolet's model is poorer beneath Cascadia than other parts [Van der Lee, personal communication], their observations are consistent with our interpretation of a hole in the slab.

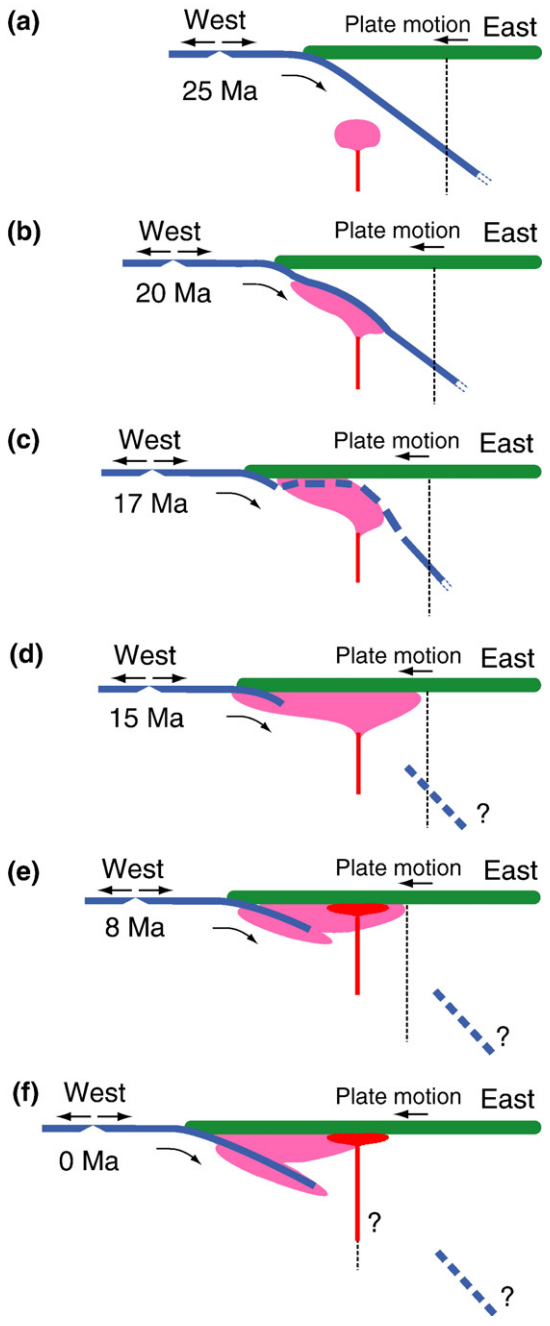

Fig. 4. Proposed tectonic model for the interaction between the subducting Juan de Fuca Plate (blue) and the Yellowstone plume head (pink). Snapshots in time are shown as: (a) 25 Ma, the Yellowstone plume is approaching the subducted Juan de Fuca plate; (b) 20 Ma, the plume head has intersected the Juan de Fuca plate and preferentially flowed westwards along the base of the slab; (c) at 17 Ma, the plume head has punched through the Juan de Fuca plate, destroyed a larger portion of the slab and caused the volcanism at the surface; (d) 15 Ma, the plume head material spreads out in a larger region at the base of the lithosphere; (e) 8 Ma, the subducting slab drags the remnant plume head material down into the mantle; (f) at present, the hot material from the remnant plume head has been brought to greater depth by the ongoing subducting slab. The vertical dashed line indicates the progression of the current Yellowstone Caldera to the west. The red plume stem represents a hypothetical Yellowstone plume since the arrival of the plume head (pink). Note: this model builds on the tectonic models proposed by Geist and Richards (1993) and Pierce et al. (2000).

The low velocity body beneath the slab in our V_s model is a feature not commonly observed beneath subducting slabs. The amplitude of the low velocity anomaly is estimated to be ~3% when the damping and smoothing effects of the inversion are taken into account. Michaelson and Weaver (1986) also concluded that a low velocity feature was present in their models from Washington to northern Oregon. They introduced a low velocity layer beneath the high velocity slab to account for the large delays observed at stations on the Olympic Peninsula and Oregon Coast Range. The low velocity layer they introduced was 80 km thick with 2–3% slower velocities beneath the dipping high velocity layer. This is very similar to what we observed here. Much broader low velocity zones beneath slabs have been observed in other subduction zones, such as in Tonga, Kuril, Japan, and the Izu region (e.g., Deal and Nolet, 1999; Deal et al., 1999; Hall and Spakman, 2002). However, the low velocity zones observed in these studies are diffuse encompassing large regions, not only underneath the slabs but also above them. The low velocity zones above slabs are consistent with arc volcanism caused by partial melting of the crustal component of subducted slabs as well as convection processes related with back arc spreading (Deal and Nolet, 1999; Zhao et al., 1997). However, the cause of the diffuse low velocity zones beneath slabs remains enigmatic.

We propose that the low velocity material beneath the Juan de Fuca slab is the remnant plume head material that has been dragged down by the subducting slab for the last 17 Ma. The plume head is estimated to be 100–300 °C hotter than the surrounding asthenosphere (Hill et al., 1992), and the time scale for cooling a plume head is of order hundreds of millions of years due to its thickness (100 to 200 km) (Hill et al., 1992). Thus the plume head material is expected to have a low velocity anomaly of 1–3%, comparable with the amplitude of the low velocity body we observed beneath the Juan de Fuca slab. Davies and Stevenson (1992) showed that a subducting slab can drag mantle material beneath the slab down with it. An experimental convection study also shows the possibility that the plume head material can be dragged down with cold downwellings (Davaille et al., submitted for publication). This high temperature low velocity body may also be partially responsible for some of the unusual characteristics of the Juan de Fuca subduction zone. The absence of a Wadati–Benioff zone of earthquakes all along the Cascadia is particularly clear beneath Oregon, east of the McDermitt Caldera where the plume head is proposed to have impacted.

To summarize our interpretation, Fig. 4 shows a tectonic reconstruction of our proposed model for the evolution of subduction beneath western North America and the interaction of the slab with a plume. We build on tectonic models proposed by Geist and Richards (1993) and Pierce et al. (2000). When the rising plume head (Fig. 4a) reaches the base of the continuous Juan de Fuca slab it begins to spread laterally. Based on geometric considerations, the buoyant plume material would spread preferentially upwards and westwards along the base of the plate while traction with the subducting plate pulls some plume head material down (Fig. 4b). At ~17 Ma, the plume head had punched through the slab, breaking up much of the subducted oceanic lithosphere, and impacted the North American continent initiating the broad voluminous volcanism in the region (Fig. 4c). Part of the plume head would spread westward (Fig. 4d) possibly as far as the Juan de Fuca Ridge (Hill et al., 1992; Parsons et al., 1994). The continuing subduction of the Juan de Fuca slab then drags the remnant plume head material down deeper into the mantle (Fig. 4e), resulting in the low velocity body imaged today (Fig. 4f). We note that the only direct evidence for a mantle plume head is the unusual low velocity layer beneath the slab today. This feature could be explained by any mechanism providing a large scale upwelling of high temperature material. However, if such a plume head impacted the North American lithosphere around this time, it would explain our observations of the Juan de Fuca plate.

5. Conclusions

Our JdF07-S and -P models image the Juan de Fuca plate as a high velocity anomaly dipping into the mantle east of the Cascades beneath Oregon. The slab reaches ~400 km depth with a dip of ~50° to the east and a thickness of ~75 km. After taking into account damping, smoothing, and imperfect ray coverage in the inversion, the actual amplitude of the velocity anomaly associated with the slab is likely ~3.8% for V_s and 1.8% for V_p. Resolution tests show that we are able to resolve any slab to a depth of ~600 km where the slab is expected to have high S-wave velocity anomalies of ~2% to 4%. Thus the abrupt end to the slab at ~400 km in our tomographic images suggests that the slab stops at that depth. We also image a layer of low velocity immediately beneath the slab extending to a depth of at least 575 km. This layer has a similar geometry as the slab: a dip of ~50°E and a thickness of ~75 km. The amplitude of this low velocity anomaly is estimated to be up to ~3% for V_s. Resolution tests show that the low velocity layer is required by data and is not an artifact of the inversion.

Using the relative plate motion between the Juan de Fuca plate and the North America Plate (HS3-NUVEL1A), the estimated total length of the slab subducted to the east in the last 17 Ma is ~480 km. This is less than the total

imaged slab length of ~660 km from the present trench in an east–west direction. Therefore, the bottom edge of the slab we observe today was east of the trench around 17 Ma. Assuming similar slab geometry to today, the ~180 km length of slab would reach a depth of ~60 km, comparable to the likely thickness of the continental lithosphere. We propose that the absence of the slab below 400 km depth today is due to the arrival of the Yellowstone plume head around 17 Ma, which destroyed the Juan de Fuca slab at depths greater than the thickness of the continental lithosphere. As the plume head material would spread westward beyond the trench possibly as far as the Juan de Fuca Ridge, traction with the subducting plate would then pull some plume head material down into the mantle. We image this material as the low velocity layer beneath the slab in our JdF07-S model. The observed low V_s anomaly of up to 3% is comparable with what expected for plume head material 100–300 °C hotter than the surrounding asthenosphere. Finally, this hot remnant plume head material beneath the slab would warm the slab and may therefore reduce its strength and the ability to generate earthquakes. This may be partly responsible for the absence of a Wadati–Benioff zone associated with the subduction of the Juan de Fuca plate.

Acknowledgements

We thank the people who assisted us in the deployment of OATS: Neal Lord, Lee Powell, Robert Pyzalski, Andrew Lockman, and William Unger from the University of Wisconsin; John Nabelek and Anne Trehu from Oregon State University, and all the land owners who hosted our stations for 3 yr. We thank Robert B. Smith for a very helpful review. We thank Gene Humphreys for allowing us using data from their deployment at Wallowa Mountain. We also use data from Berkeley Digital Seismograph Network, Cascade Chain Volcano Monitoring, Global Seismograph Network, Laser Interferometer Gravitational-Wave Experiment, Princeton Earth Physics Project-Indiana, Pacific Northwest Regional Seismic Network, USArray Transportable Network, University of Oregon Regional Network, and the United States National Seismic Network. The IRIS DMC provided seismic data. This work was supported by the NSF (EAR-0539987). The figures were produced with SAC and GMT (Wessel and Smith, 1995). This is Berkeley Seismological Laboratory contribution number 07-14.

References

Allen, R.M., Nolet, G., Morgan, W.J., Vogfjord, K., Bergsson, B.H., Erlendsson, P., Foulger, G.R., Jakobsdottir, S., Julian, B.R., Pritchard, M., Ragnarsson, S., Stefansson, R., 2002. Imaging the mantle beneath Iceland using integrated seismological techniques. J. Geophys. Res.-Solid Earth 107, 2325. doi:10.1029/2001JB000595.

Bijwaard, H., Spakman, W., Engdahl, E.R., 1998. Closing the gap between regional and global travel time tomography. J. Geophys. Res.-Solid Earth 103, 30055–30078.

Bostock, M.G., VanDecar, J.C., 1995. Upper-mantle structure of the northern Cascadia subduction zone. Can. J. Earth Sc. 32, 1–12.

Bostock, M.G., Hyndman, R.D., Rondenay, S., Peacock, S.M., 2002. An inverted continental Moho and serpentinization of the forearc mantle. Nature 417, 536–538.

Cammarano, F., Goes, S., Vacher, P., Giardini, D., 2003. Inferring upper-mantle temperatures from seismic velocities. Phys. Earth Planet. Inter. 138, 197–222.

Camp, V.E., Ross, M.E., 2004. Mantle dynamics and genesis of mafic magmatism in the intermontane Pacific Northwest. J. Geophys. Res.-Solid Earth 109.

Christiansen, R.L., Yeats, R.S., 1992. Post-Laramide geology of the U.S. Cordilleran region. In: Burchfiel, B.C., Lipman, P.W., Zoback, M.L. (Eds.), The Cordilleran Orogen: Conterminous U.S. G-3. Geological Society of America, Boulder, Colorado, pp. 261–406.

Christiansen, R.L., Foulger, G.R., Evans, J.R., 2002. Upper-mantle origin of the Yellowstone hotspot. Geol. Soc. Amer. Bull. 114, 1245–1256.

Davaille, A., Limare, A., Vidal, V., Vatteville, J., Le Bars, M., Carbonne, C., Bienfait, G., Imaging isotherms in viscous convecting fluids, Exp. Fluids (submitted for publication).

Davies, J.H., Stevenson, D.J., 1992. Physical model of source region of subduction zone volcanics. J. Geophys. Res.-Solid Earth 97, 2037–2070.

Deal, M.M., Nolet, G., 1999. Slab temperature and thickness from seismic tomography 2. Izu–Bonin, Japan, and Kuril subduction zones. J. Geophys. Res.-Solid Earth 104, 28803–28812.

Deal, M.M., Nolet, G., van der Hilst, R.D., 1999. Slab temperature and thickness from seismic tomography 1. Method and application to Tonga. J. Geophys. Res.-Solid Earth 104, 28789–28802.

Draper, D.S., 1991. Late Cenozoic bimodal magmatism in the northern Basin and Range Province of southeastern Oregon. J. Volcanol. Geotherm. Res. 47, 299–328.

Flueh, E.R., Fisher, M.A., Bialas, J., Jonathan, R., Klaeschen, D., Kukowski, N., Parsons, T., Scholl, D.W., ten Brink, U., Trehu, A.M., Vidal, N., 1998. New seismic images of the Cascadia subduction zone from cruise SO108-ORWELL. Tectonophysics 293, 69–84.

Geist, D., Richards, M., 1993. Origin of the Columbia Plateau and Snake River plain — deflection of the Yellowstone plume. Geology 21, 789–792.

Goes, S., Govers, R., Vacher, P., 2000. Shallow mantle temperatures under Europe from P and S wave tomography. J. Geophys. Res.-Solid Earth 105, 11153–11169.

Grand, S.P., 2002. Mantle shear-wave tomography and the fate of subducted slabs. Philos. Trans. — Royal Soc., Math. Phys. Eng. Sci. 360, 2475–2491.

Gripp, A.E., Gordon, R.G., 2002. Young tracks of hotspots and current plate velocities. Geophys. J. Int. 150, 321–361.

Hall, R., Spakman, W., 2002. Subducted slabs beneath the eastern Indonesia–Tonga region: insights from tomography. Earth and Planet. Sci. Lett. 201, 321–336.

Harris, R.A., Iyer, H.M., Dawson, P.B., 1991. Imaging the Juan Defuca Plate beneath southern Oregon using teleseismic P-wave residuals. J. Geophys. Res.-Solid Earth 96, 19879–19889.

Hill, R.I., Campbell, I.H., Davies, G.F., Griffiths, R.W., 1992. Mantle plumes and continental tectonics. Science 256, 186–193.

Humphreys, E.D., Dueker, K.G., Schutt, D.L., Smith, R.B., 2000. Beneath Yellowstone: evaluating plume and nonplume models using teleseismic images of the upper mantle. GSA Today 10, 1–7.

Jordan, B.T., 2005. Age-progressive volcanism of the Oregon HIgh Lava Plains: overview and evaluation of tectonic models. In: Foulger, G.R., Natland, J.H., Presnall, D.C., Anderson, D.L. (Eds.), Plates, Plumes, and Paradigms 388. Geological Society of America Special Paper, pp. 503–515.

Jordan, B.T., Grunder, A.L., Duncan, R.A., Deino, A.L., 2004. Geochronology of age-progressive volcanism of the Oregon High Lava Plains: implications for the plume interpretation of Yellowstone. J. Geophys. Res. 109. doi:10.1029/2003JB002776.

Marone, F., Romanowicz, B., 2007. Non-linear crustal corrections in high-resolution regional waveform seismic tomography. Geophys. J. Int. 170, 460–467.

McCrory, P.A., Blair, J.L., Oppenheimer, D.H., Walter, S.R., 2006. Depth to the Juan De Fuca slab beneath the Cascadia subduction margin-A 3-D model for sorting earthquakes. U.S. Geological Survey, Data Series 91, Version 1.2.

Michaelson, C.A., Weaver, C.S., 1986. Upper mantle structure from teleseismic P-wave arrivals in Washington and northern Oregon. J. Geophys. Res.-Solid Earth and Planets 91, 2077–2094.

Parsons, T., Thompson, G.A., Sleep, N.H., 1994. Mantle plume influence on the neogene uplift and extension of the United-States Western Cordillera. Geology 22, 83–86.

Pierce, K.L., Morgan, W.J., 1992. The track of the Yellowstone hotspot: volcanism, faulting, and uplift. In: Link, P.K., Kuntz P.L.B., M.A. (Eds.), Regional Geology of Eastern Idaho and Western Wyoming 179. Geological Society of America Memoir, pp. 1–53.

Pierce, K.L., Morgan, L.A., Saltus, R.W., 2000. Yellowstone Plume Head: Postulated Tectonic Relations to the Vancouver Slab, Continental Boundaries and Climate. 39 pp.

Rasmussen, J., Humphreys, E., 1988. Tomographic image of the Juan-Defuca-Plate beneath Washington and western Oregon using teleseismic P-wave travel-times. Geophys. Res. Lett. 15, 1417–1420.

Severinghaus, J., Atwater, T., 1990. Cenozoic geometry and thermal state of the subducting slabs beneath western North America. In: Wernicke, B.P. (Ed.), Basin and Range Extensional Tectonics Near the Latitude of Las Vegas, Nevada. Geological Society of America Memoir, vol. 176. Boulder, Colorado.

Shelly, D.R., Beroza, G.C., Zhang, H.J., Thurber, C.H., Ide, S., 2006. High-resolution subduction zone seismicity and velocity structure beneath Ibaraki Prefecture Japan. J. Geophys. Res.-Solid Earth 111.

Smith, R.B., Braile, L.W., 1994. The Yellowstone hotspot. J. Volcanol. Geotherm. Res. 61, 121–187.

Trehu, A.M., Lin, G.B., Maxwell, E., Goldfinger, C., 1995. A seismic-reflection profile across the Cascadia subduction zone offshore central Oregon — new constraints on methane distribution and crustal structure. J. Geophys. Res.-Solid Earth 100, 15101–15116.

Vandecar, J.C., Crosson, R.S., 1990. Determination of teleseismic relative phase arrival times using multi-channel cross-correlation and least-squares. Bull. Seismol. Soc. Am. 80, 150–169.

vanderLee, S., Nolet, G., 1997. Seismic image of the subducted trailing fragments of the Farallon plate. Nature 386, 266–269.

Waite, G.P., Smith, R.B., Allen, R.M., 2006. V-P and V-S structure of the Yellowstone hot spot from teleseismic tomography: evidence for an upper mantle plume. J. Geophys. Res.-Solid Earth 111.

Wessel, P., Smith, W.H.F., 1995. New version of the Generic Mapping Tools released. EOS, Trans. Am. Geophys. Un. 76, 329.

Wilson, D.S., 1988. Tectonic history of the Juan-De-Fuca-Ridge over the last 40 million years. J. Geophys. Res.-Solid Earth and Planets 93, 11863–11876.

Yuan, H.Y., Dueker, K., 2005. Teleseismic P-wave tomogram of the Yellowstone plume. Geophys. Res. Lett. 32.

Zhao, D.P., Christensen, D., Pulpan, H., 1995. Tomographic Imaging of the Alaska Subduction Zone. J. Geophys. Res.-Solid Earth 100, 6487–6504.

Zhao, D.P., Xu, Y.B., Wiens, D.A., Dorman, L., Hildebrand, J., Webb, S., 1997. Depth extent of the Lau back-arc spreading center and its relation to subduction processes. Science 278, 254–257.